Published in "Galactic and Extragalactic Radio Astronomy", 1974, eds. G.L. Verschuur and K.I. Kellerman.

For a PDF version of the article, click here.

MAPPING NEUTRAL HYDROGEN IN EXTERNAL GALAXIES

Melvyn C. H. Wright

Table of Contents

11.1. INTRODUCTION

11.1.1. Hydrogen Distribution and Kinematics

Hydrogen is the building material for stars and galaxies, and a study of its distribution and kinematics in external galaxies is essential to understanding the dynamics and evolution of these objects. Much can be learned by comparing the overall or integral properties of different galaxies, but an understanding of the detailed distribution of neutral hydrogen in a galaxy can be derived only from a high-resolution map.

The Magellanic Clouds were the first extra-galactic objects observed in the 21-cm line (Kerr, Hindman, and Robinson, 1954). The large angular extent of these objects enabled a detailed map to be made of the neutral hydrogen density and velocity distribution across the Clouds. The aim of observations today is to make similarly detailed maps for ordinary spiral and irregular galaxies.

The story of mapping neutral hydrogen in external galaxies is one of a continuing quest for angular resolution, but we shall first briefly review the classification and properties of the galaxies we will be talking about.

11.1.2. Classification Systems

Normal galaxies have been classified under several schemes. The Hubble classification (Sandage, 1961), based on the morphological features visible on blue-sensitive plates, is perhaps the most widely used. This scheme, which divides spiral galaxies into three classes - Sa, Sb, Sc - depending on the openness of the spiral features, has been extended by Holmberg (1958) and the de Vaucouleurs (1964), and has much to recommend it, in that it would seem to represent a real separation in terms of the evolutionary parameters (e.g., fractional hydrogen content) of the galaxies. This is not to say that the series is an evolutionary sequence. Indeed, unless there can be considerable accretion of mass by a galaxy it would appear impossible for evolution to take place along the series from the irregular and Sc galaxies (which, on average have the highest fractional hydrogen content) to the more massive Sa spirals and ellipticals.

Equivalent classifications under these morphological systems are set out in the introduction to the de Vaucouleurs' (1964) *Reference Catalogue of Bright Galaxies.*

The Morgan (Yerkes) (1958, 1959) classification is a valuable complementary alternative to the Hubble classification. In this system the parameter *a - k* denotes increasing central concentration of light, while the luminosity is progressively from A- to K-type stars (Morgan and Mayall, 1957). Although the early-type (Sa) spirals tend to have a higher degree of central condensation and the Hubble type correlates well with the integrated color of galaxies (Holmberg, 1958), there is not a one-to-one correspondence between the Hubble and Morgan classifications. A further classification system for late-type spirals (Sc and Sb) is that of van den Bergh (1960a, 1960b), based on a strong correlation between the absolute luminosity and the degree of development of the spiral arms.

These classification systems are interrelated, but not exactly equivalent, and each is useful in discussing the properties of spiral galaxies.

11.2. INTEGRAL PROPERTIES OF GALAXIES

The overall characteristics of a galaxy are determined by its so-called integral properties, which include the morphological form under some classification system, color, total mass, luminosity, hydrogen mass, HII region abundance, radio continuum power, etc. By studying the correlations among these parameters we hope to learn something of the evolution of galaxies and the reasons for their different morphological forms.

Surveys of external galaxies in the 21-cm line have been made by a number of authors, and there are several excellent reviews of the integral properties of galaxies (e.g., Roberts, 1967, 1969). We shall merely note here some of the established trends of the integral properties.

11.2.1. The Data

a) Hydrogen Mass

The mass of neutral hydrogen galaxy is derived from its 21-cm emission spectrum. The surface density (atom cm^{-2}) of hydrogen radiating in a 1 km sec^{-1} interval is given by

$$n_\upsilon = 1.823 \times 10^{18} T_s \tau_\upsilon \qquad (1)$$

where T_s is the spin temperature of the gas, and τ_v the optical depth (see, for example, Chapter 2).

T_s is assumed here to be constant along Galactic and Extra-Galactic Radio Astronomy the column of radiating gas. If the gas is optically thin ($T_B << T_s$), then the surface density is given by

$$n = 1.823 \times 10^{18} \int_{\text{velocity}} T_B dV \tag{2}$$

and the total number of atoms, *N*, is obtained by integrating the surface density across the galaxy

$$N = 1.823 \times 10^{18} \int_{\text{galaxy}} dS \int_{\text{velocity}} T_B dV \tag{3}$$

An element of surface area *dS* is related to the distance D by $dS = D^2 \, d\Omega$. Thus the number of atoms is proportional to D^2 and the integrated line flux is given by

$$N = 1.823 \times 10^{18} D^2 \int\int T_B dV \, d\Omega \tag{4}$$

or in convenient units,

$$\frac{M}{M_\odot} = 2.356 \times 10^5 D^2 \int S_\nu dV \tag{5}$$

where *D* is in Mpc, S_v in flux units [1], and *dV* in km sec^{-1}.

The assumption of small optical depth may be invalid, particularly where the velocity dispersion of the gas is small or the line of-sight thickness is large owing to the high inclination of the galaxy. In this case the mass of neutral hydrogen derived above is a lower limit. Also, the variation of T_s (known to occur in our galaxy) makes the mass a lower limit from another point of view, as some of the hydrogen will be in cold clouds of substantial opacity. It is tacitly assumed that there is no interaction between radio continuum and line radiation. Epstein (1964) has considered these problems for different cases.

b) Total Masses

The masses of spiral galaxies are estimated by assuming that the galaxies are in rotational equilibrium. The line-of-sight velocity of some component of the galaxy - usually neutral hydrogen or ionized hydrogen, oxygen, and nitrogen - can be measured by the Doppler shift of its corresponding line emission. In the case of irregular galaxies (or for low-resolution neutral hydrogen measurements) the mass of the galaxy can be estimated (e.g., Bottinelli et al., 1968) directly from the measured velocity dispersion using the virial theorem (Chandrasekhar, 1942). More usually, for spiral galaxies a rotation velocity is estimated as a function of radius and a mass is derived from a model for the centrifugal equilibrium of the gas. The basic equation is of the same form in either case and the estimated mass scales linearly with the assumed distance to the galaxy. Assuming that the galaxy is a plane rotating disk in centrifugal equilibrium, a simple Keplerian estimate of the total mass is obtained as $M_T = (rv^2 / G)$, where the maximum rotational velocity v occurs at a radius r. In convenient units this gives

$$M_T = 6.8 \times 10^4 \times r[\text{min arc}] \times D[\text{Mpc}] \times v([\text{km sec}^{-1}])^2 M_{\odot} \quad (6)$$

As discussed in more detail in Sections 11.5 and 11.6, the neutral hydrogen data usually have poor angular resolution and the total mass must be derived from a model for the rotation curve. The optical data, however, have high angular resolution and provide a detailed mass distribution, but only out to the limiting radius of the emission lines (e.g., Burbidge, Burbidge, and Prendergast, 1963). There is some difficulty, then, in comparing masses derived from optical and radio data.

c) Luminosity

The measured luminosity of a galaxy increases with the area of the photographic image integrated. The Holmberg (1958) system of luminosities and diameters of galaxies provides a well-defined measurement down to a sky-brightness-limited isophote of $26.^m5$ per square second arc. The measured luminosities and colors on the UBV system can be corrected for an average galactic extinction by -0.25 cosec (latitude) and for inclination of the observed galaxy. The absolute luminosity of a galaxy is usually quoted in units of the solar luminosity and of course scales as the square of the assumed distance.

d) Selection Effects

Observational requirements force a selection of galaxies which may affect the correlations described below. The neutral hydrogen measurements are biased toward the late-type (Sc and Irr) galaxies and optical measurements of rotation curves tend to be of intrinsically bright galaxies. Upper limits for the HI-to-total mass ratio of ≈ 0.1% have been established for several elliptical galaxies (Bottinelli et al. 1973), and we shall confine ourselves in what follows to the spiral and irregular galaxies.

---

[1] 1 flux unit = 10^{-26} Wm^{-2} Hz^{-1} Back.

11.2.2. Correlations

a) Mass Luminosity

The masses and luminosities of spiral and irregular galaxies cover about four orders of magnitude, and a plot of mass against luminosity (e.g., Roberts, 1969) shows that the brighter galaxies are more massive. The mass-to-light ratio is approximately constant with one order of magnitude dispersion ($M / L \approx 4$ solar units $M_{\odot} / L_{\odot}$). There is no separation according to structural type in the mass-luminosity diagram, except in the case of the irregulars, which tend to be low-mass intrinsically faint systems. Without the irregulars the relationship between mass, luminosity, and morphological type is not obvious.

b) Hydrogen Mass Luminosity

The distance to an external galaxy is generally ill-determined and distance-independent parameters are of great value in establishing correlations between the integral properties of galaxies. The neutral hydrogen-to-luminosity ratio, M_{H} / L, is such a parameter and tends to be higher in the bluer later-type galaxies (e.g., Epstein, 1964). The neutral hydrogen content is itself correlated with the luminosity, and these two correlations probably signify that star formation is proceeding rapidly in galaxies containing more hydrogen.

c) Fractional Hydrogen Content

A plot of neutral hydrogen mass versus total mass (e.g., Roberts, 1969) again shows a correlation, but one which is highly dependent on the presence of the low-mass irregular systems. There is a clear relationship between the fractional hydrogen content and the structural type. The HI content ranges from 1 to 2% hydrogen in the Sa spirals to over 30% in the irregular systems. This is the most striking relationship in the integral properties of galaxies and probably indicates that the early-type spirals are more evolved than the late-type spirals and irregulars.

d) Ionized Hydrogen

Except for the nearest galaxies, ionized hydrogen has been discussed only in terms of large HII regions. Sersic (1960) has made a survey of HII regions in 66 galaxies and finds that the mean size of the three largest HII regions increases progressively with neutral hydrogen content from the earlier types to the Sc^{-} galaxies and then decreases again in the dwarf Sc and irregulars. Hodge (1967) has cataloged the positions of HII regions in 66 galaxies and finds in an analysis of 25 of these (Hodge, 1969) that the distribution of HII regions within a galaxy tends to be a function of the morphological type, possibly indicating a difference in the state, or rate of evolution, of the galaxies.

e) Radio Continuum

Normal spiral galaxies are sources of nonthermal radio continuum, with flux densities of typically 0.1 to 1 flux unit, at 408 MHz. The optical and radio luminosities of spiral galaxies are closely correlated and recent data (Cameron, 1971) has shown that this correlation is even stronger for the restricted set of galaxies of Morgan type f. The radio continuum power is better correlated with the van den Bergh and Morgan classifications than with the Hubble type. The correlation with the van den Bergh classification and hence with spiral arm development is particularly interesting in the light of recent maps of spiral galaxies, e.g., M31 (Pooley, 1969) and M51 (Mathewson, et. al., 1972), showing that spiral arms are sources of radio continuum emission.

11.3. MAPPING HI IN GALAXIES

11.3.1. Density Distribution

a) Extent of Distribution

The integral properties of galaxies have revealed several interesting correlations of total mass and hydrogen abundance with morphological type, but have not answered the question as to why the different morphological types exist. We can hope to gain insight into this, and the question of evolution and star formation in galaxies, only if we know more details of the structure and distribution of the different components of a galaxy. Particularly lacking in this respect is a detailed knowledge of the distribution of the neutral hydrogen, the most basic component of a galaxy. The mapping of neutral hydrogen in external galaxies allows us to find such things as:

1. The overall form of the HI distribution, how this compares with that of the total mass distribution, and where the highest hydrogen concentrations are.
2. The extent of the hydrogen distribution. Is it coextensive with the luminous population of a galaxy? How sharp are its boundaries ?
3. Neutral hydrogen wings, bridges between galaxies and companions or satellites with the same sort of relationship as the Magellanic Clouds are believed to have to the Milky Way.

b) Spiral Arms

The above questions can be answered with fairly limited resolution. With higher resolution we may comment further on whether the neutral hydrogen has the form of spiral arms and if these are coincident with the spiral arms defined by the bright HII regions or displaced from them.

A detailed correlation can be made of the surface densities of the young O and B stars, the HII regions they excite, and the neutral hydrogen from which they have been formed. This is a very important field, for in our galaxy the situation is confused by the complex velocity-distance relationship. In an external galaxy one has an overall view of the distribution of the different components.

11.3.2. Velocity Distribution

a) Line-of-Sight Velocity

Observations of neutral hydrogen are usually made with a multi-channel spectrometer so that the frequency or velocity distribution of the line radiation is also determined. Neutral hydrogen-line radiation arises from a forbidden transition, and the low-transition probability implies a small natural width of the line (5×10^{-16} Hz). The observed width of the line is therefore due to Doppler broadening (-4.74 kHz / km sec^{-1}) at the line rest frequency of 1420.4 MHz.

The line broadening is partly due to random and thermal motions in the gas, but is mainly due to larger-scale motions of the gas. In a spiral galaxy the dominant motion is one of rotation, although expansion motions and other "peculiar" velocities are of great interest. The line-of-sight velocity of the neutral hydrogen in any portion of the galaxy can be measured as a Doppler shift, and with sufficient angular and frequency resolution we observe different Doppler shifts across the face of the galaxy. The line-of-sight velocity is interpreted in terms of the rotation, expansion, and other velocities in the galaxy, which is assumed to have a plane rotating disk geometry.

b) Isovelocity Contours

The observed line-of-sight velocity $u(r, \phi)$ of hydrogen with azimuthal coordinates (r, ϕ) in a plane galaxy inclined at an angle i to the plane of the sky is given by

$$\begin{aligned} u(r, \phi) = {} & v_0 + v(r, \phi) \sin i \cos \phi \\ & + w(r, \phi) \sin i \sin \phi + z(r, \phi) \cos i \end{aligned} \qquad (7)$$

where v_0 is the systemic velocity, $v(r, \phi)$ the tangential velocity (including both the rotation of the galaxy and "peculiar" streaming and random components), $w(r, \phi)$ a radial velocity in the plane of the galaxy, and $z(r, \phi)$ a velocity out of the plane of the galaxy. A complete analysis of the kinematics of a galaxy should include all these effects. If the motion of the hydrogen in a galaxy is one of pure rotation, then the lines of constant observed radial velocity will be the lines

$$v(r) \cos \phi = \text{constant} \qquad (8)$$

A plot of $v(r)$ against radius r is called the rotation curve for the galaxy and typically has the form shown in Figure 11.1. For a rotation curve of this form the lines of constant observed velocity (the *isovelocity contours*) will have the form shown in Figure 11.2. Where the rotation is solid-body, i.e., $v(r) \propto r$, the isovelocity contours are parallel to the minor axis of the galaxy. The region of solid-body rotation is shown enclosed by the dashed line in Figure 11.2. Other systematic motions of the galaxy have characteristic isovelocity contours; e.g., the addition of an expansion, $w(r) \propto r$, gives isovelocity contours in the solid-body region inclined at an angle to the minor axis. Closed isovelocity contours are produced by the region of the rotation curve where the rotation velocity is decreasing with radius.

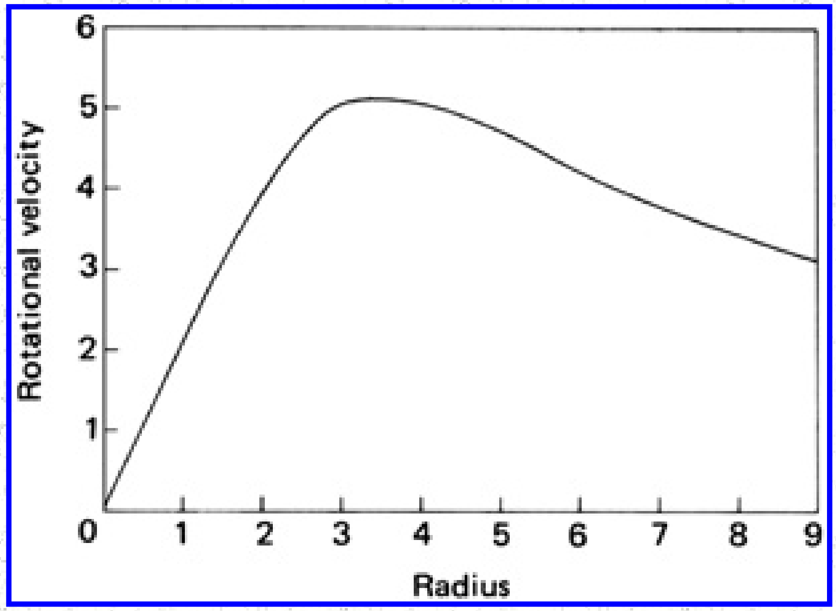

Figure 11.1. Model rotation curve showing (1) solid-body rotation out to 3 units radius, (2) constant velocity region between radii 3 and 4, (3) region of decreasing rotation velocity. (M. C. H. Wright.)

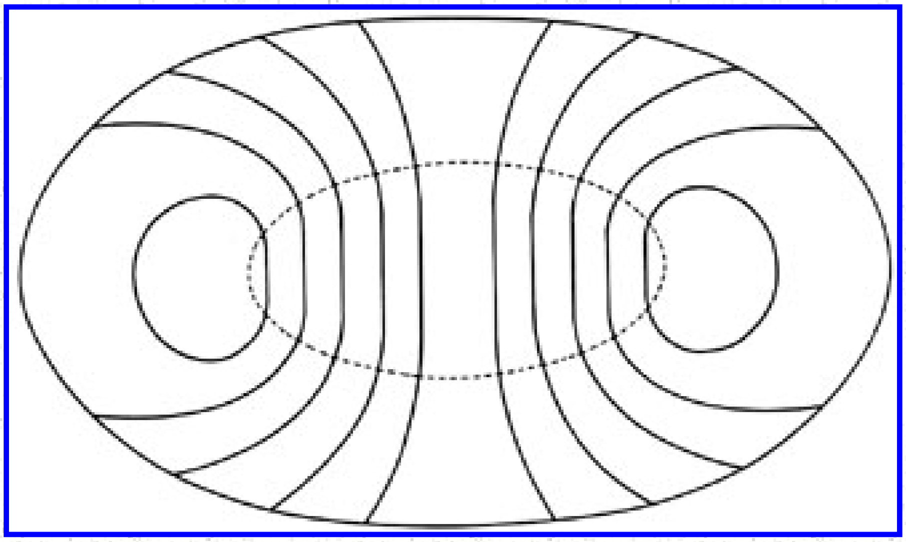

Figure 11.2. Isovelocity contours (lines of constant line-of-sight velocity) in a rotating galaxy. The contours are drawn at intervals of the units of velocity in Figure 11.1 The region of solid-body rotation is shown enclosed by the dashed line. [M. C. H. Wright, Astrophys. J. (1971) 166:455.]

c) Interpretation

From the velocity information we can investigate

1. rotation of the galaxy and the shape of the rotation curve
2. the total mass and a mass distribution for the galaxy
3. angular momentum distribution
4. velocity dispersion of the gas and hence an estimate of the thickness of the neutral hydrogen layer
5. peculiar velocities, expansion motions
6. perturbations due to spiral arms, streaming motions, and density waves.

The above list has been compiled in order of increasing observational difficulty. Observation of the spiral arms and their perturbations requires the highest resolution and sensitivity and is the subject of current research.

The highest physical resolution so far obtained has been the observations of the Magellanic Clouds with the 210-foot Parkes dish, where the half-power bandwidth is equivalent to about 200 pc at the distance of the clouds. In order to obtain comparable resolution in the nearest spiral galaxies an angular resolution of the order of 1 minute arc is required and we must resort to aperture synthesis techniques. Aperture synthesis in general is discussed in Chapter 10, and its application to spectral-line work is discussed in Section 11.6, but let us first see what has been achieved with single dish measurements.

11.4. OBSERVATIONS WITH A SINGLE DISH

11.4.1. Observing Procedure

The radiometer system commonly used consists of a multi-channel (or swept-frequency) receiver, whose overall bandwidth covers the range of velocities to be found in the observed galaxy and is centered on or near the systemic velocity of the galaxy. The receiver is frequency-switched in order to establish a reference outside the hydrogen line, or observations are made on and off the source to find a frequency baseline for the spectrum. Scans are made across the galaxy, and the intensity in each frequency channel is recorded as a function of RA and declination. The sensitivity of the frequency channels may be calibrated by observing continuum sources or by injecting broad-band noise into the system. After calibrating the data, intensity-versus-frequency (or velocity) spectra may be drawn on a grid of points on the sky. These are the basic data. Integration under all the profiles yields a map of the hydrogen emission brightness temperature. Radio continuum emission from the galaxy may be subtracted, on the assumption of little interaction with the line radiation, by using channels outside the hydrogen-line emission or by using an off-frequency observation.

Because the resolution is limited, the frequency profiles are usually single-peaked, and it is an easy process to establish a velocity at the peak, median value, or leading edge of the profile. Thus a single velocity at each grid point can be derived and a map of iso-velocity contours of the line-of-sight velocity can be plotted.

Most galaxies subtend only a few beam areas, but for the nearest galaxies there are many beam areas and the maps derived give beam-smoothed estimates of the overall hydrogen density and velocity distribution.

11.4.2. Magellanic Clouds

As already mentioned, the observations of the Magellanic Clouds with the Parkes 210-foot dish have the highest physical resolution so far attained. The Magellanic Clouds cover some 800 square degrees of sky and, at a distance of ≈ 50 kpc, are the nearest extragalactic objects to our own galaxy. A low-resolution (2.°2 beamwidth) HI survey (Hindman, Kerr, and McGee, 1963) showed that the Large and Small Clouds (LMC and SMC) are embedded in the same HI envelope. The total HI mass of the system is some 1.5×10^9 $M_\odot$; 5.4×10^8 $M_\odot$ is associated with the LMC and 4.8×10^8 $M_\odot$ with the SMC.

The 210-foot survey of the LMC (McGee and Milton, 1966) revealed 52 HI complexes of mean HI mass 4×10^6 $M_\odot$ and diameter 575 pc (≈ 1 HI atom/cc). The HI complexes are closely associated (in position and velocity) with HII regions and OB stars, but do not correlate with the stellar clusters.

Of 90 large HII regions cataloged by Henize (1956), 61 are closely associated with the HI complexes. The supergiant OB stars with measured velocities also have a high correlation in position and velocity with the HI complexes.

From an analysis of the rotation of the LMC and the position and velocity distribution of the population I objects, McGee and Milton (1966) proposed a spiral structure for the LMC. The total mass derived from rotational and random motions is greater than 6×10^9 $M_\odot$, giving the LMC a fractional hydrogen content of 5 to 9%. The 1410-MHz radio continuum also correlates well with the integrated hydrogen contours.

The neutral hydrogen distribution in the SMC is rather smooth, with three major concentrations reaching peak brightness temperatures of 150, 110, and 100°K, merging into a high-level background. This smooth distribution is in striking contrast to the clumpy distribution in the LMC. The most interesting feature of the 210-foot survey (Hindman, 1967) is the presence of what would appear to be three massive (1 to 2×10^7 $M_\odot$) expanding neutral hydrogen shells of diameter 1 to 2 kpc, which could be the result of supernova explosions. The SMC is also thought to be rotating, but is only slightly flattened. The estimated mass is 1.5×10^9 $M_\odot$, with some 30% neutral hydrogen. As in the LMC, there is a correlation between the distribution of neutral hydrogen and the bright stars. About half of the cataloged HII regions (Henize, 1956) are located in the vicinity of the three major gas concentrations.

11.4.3. Nearby Spiral Galaxies

Although the Magellanic Clouds are closest and allow the most detailed comparison of optical and radio features, it is important to also observe the external spiral galaxies which more closely resemble the Milky Way. Our galaxy is thought to have a morphological form somewhere between that of M31 and M33 (see Burke, 1967). Both of these galaxies have been mapped with 10 minutes arc resolution, equivalent to 2 kpc at a distance of 680 kpc. At this resolution the most prominent feature of the HI distribution of M31 is a deficiency of hydrogen in the central regions, with the peak hydrogen distribution in the form of a broad ring at a radius of 50 minutes are (Roberts, 1966; Gottesman and Davies, 1970). The OB star associations, HII regions, and radio continuum emission are closely correlated with the ridge of neutral hydrogen, all of which suggests that star formation is proceeding at maximum rate where the neutral hydrogen density is highest (see Section 11.7.5). There are several possibilities for the deficit of neutral hydrogen in the central regions of M31 (a feature it has in common with our galaxy and several other external galaxies; see Section 11.7.4).

A rotation curve has been derived out to 150 minutes arc from the center of M31. The computed mass distribution gives an almost constant *M*/*L* (mass-to-light) ratio (11.9$M_\odot$ / $L_\odot$) over the entire galaxy. The total mass within 150 minutes arc is some 2×10^{11} $M_\odot$, giving M31 a fractional hydrogen content of 2% - typical for an Sb galaxy. There is a marked asymmetry in the isovelocity contours of adjacent quadrants of the galaxy, and the rotation curves derived separately for the north and south of the galaxy differ in the central regions by some 30 km sec^{-1}. These asymmetries have been interpreted as a tilt in the plane of the galaxy of some 10° and could be caused by the tidal effect of the companion galaxies M32 and NGC 205 in a similar way to the suggested influence of the Magellanic Clouds on the Milky Way (Avner and King, 1967).

M33 is an Sc galaxy and has the second largest angular size in the Northern Hemisphere. At an assumed distance of 690 kpc it lies some 190 kc from M31. Observations with a 10-minutes-arc resolution (Gordon, 1971) reveal a neutral hydrogen distribution with the same overall dimensions as the Holmberg optical size (83 × 53 minutes arc). The neutral hydrogen distribution is asymmetric, with a major concentration in the south-preceding quadrant and a 10% central depression. At the extreme ends of the major axis are two companions, or wings, of the galaxy which have a very different position angle to that of the main body of the galaxy. These wings contain 10% of the total HI mass. The computed rotation curve is rather flat-topped, and the derived total mass within 60 minutes arc of the center is 2.3×10^{10} $M_\odot$. The neutral hydrogen mass is some 7% of this total. The velocities in the wings do not follow those predicted by the rotation curve, and a consistent interpretation is that the wings are stable gaseous companions gravitationally bound to M33 rather like the Magellanic Clouds are to our galaxy. M33 is discussed in greater detail in Section 11.7.1.

11.4.4. Galaxies with Smaller Angular Diameters

With more distant galaxies, where the beam size is comparable with the angular diameter of the galaxy, it is still possible to measure the line profile and estimate the mass of neutral hydrogen. The velocity width of the profile allows an estimate of the rotation or random velocities within the galaxy and, with the usual assumption of gravitational equilibrium, the mass of the galaxy may be estimated.

When the hydrogen distribution subtends 2 or 3 beamwidths, an estimate of the large-scale HI distribution may be made and compared with the optical features. An example of this sort of observation is the work done by the Meudon group with the Nançay radio-telescope. This instrument has a beamwidth of 4 minutes arc E-W by $\gtrsim$ 24 minutes arc N-S at 21-cm, which allows an estimate of the E-W hydrogen distribution. Using this instrument Bottinelli (1971) finds that the hydrogen distribution is asymmetrical with respect to the optical distribution in about 40% of the galaxies observed. The ratio of the neutral hydrogen diameter to the optical diameter [measured on the Holmberg (1958) system] is observed to be a function of the morphological type, increasing toward the later-type galaxies. This characteristic gives a mean HI surface density independent of the galactic type. Details of the neutral hydrogen distribution may be deduced through a model-fitting procedure, and Bottinelli finds that a ring-like model for the HI distribution (as in M31) is consistent with about 30% of the galaxies observed and that the neutral hydrogen seems to be more strongly concentrated toward the center in the early-type galaxies.

11.4.5. Model Fitting

a) HI Distribution and Rotation Curve

The technique of taking a model distribution for a source and smoothing it by the observing beam is well known. We can do rather better with line observations, as the distribution of HI in a particular velocity range is a function of both the density and velocity distribution of the gas. For a rotating galaxy with isovelocity contours, as in Figure 11.2, observations in the different velocity channels are essentially of the regions delimited by the isovelocity contours. The shape of these is determined by the rotation curve and other motions in the galaxy. Profiles of brightness temperature versus velocity may be generated from a model for the rotation curve and the neutral hydrogen distribution. The generation of model profiles is usually performed with a digital computer and many input models can be tried. The HI distribution and rotation curve, which give profiles that most resemble the observed profiles, are to be preferred. The chief drawback to this procedure is that there must always be two multi-parameter inputs: the rotation curve and the hydrogen distribution. These interact in the generation of the model profiles and it is usually possible to get a good fit to the observed profiles with more than one input model.

b) Minor Axis Profiles

The region radiating in a small velocity range about the systemic velocity of a rotating galaxy lies close to the minor axis (see Figure 11.2). In a direction orthogonal to the minor axis the region observed may be much narrower than the beamwidth. With limited resolution the shape of the hydrogen distribution in a small velocity range about the systemic velocity (*viz.*, the minor axis profile) is often observed to be double-peaked or flat-topped. This observation has led to the suggestion (Roberts, 1967) that the distribution of hydrogen along the minor axis is also double-peaked and that a ring-shaped distribution of hydrogen, as in M31, is a common feature of the HI distribution in external galaxies. Consideration of Figure 11.2 shows that the shape of the minor axis profile is a function of both the distribution of HI along the minor axis and the shape of the isovelocity contours defining the minor axis region observed.

In M31 the neutral hydrogen distribution along the minor axis is double-peaked in the integrated neutral hydrogen distribution as well as in a small velocity range centered on the systemic velocity, and the description of the overall distribution of HI as a ring is a good one. M33 has a similar double-peaked minor axis profile in a small velocity range, but this is due to the shape of the isovelocity contours, and the HI distribution is really rather flat-topped. It remains to be seen from higher-resolution observations whether a ring is a good general description of the neutral hydrogen distribution in external galaxies (see Section 7.3).

c) Mass Derivations

In many cases the internal motion of an external galaxy is well approximated by a rotation law, $v(r)$, and if we assume that the rotating galaxy is in dynamic equilibrium under self-gravitation, it is possible to derive a mass distribution from the rotation law. Several schemes have been used for calculating a mass distribution from the rotation curve. Most mass derivations based on optically measured rotation curves have used a mass model of the form of concentric spheroids developed by Burbidge, Burbidge, and Prendergast (1963). The mass is calculated by fitting a polynomial to the rotation curve, and substituting this into the equation for the equilibrium of the concentric spheroids to derive the density as a function of radius. Use of a polynomial with more than five or six terms produces unrealistic oscillations in the rotation curve, and the calculated mass distribution is not particularly sensitive to the number of terms in the polynomial used.

Many spiral galaxies are highly flattened and a variable density disk is a good model. Model rotation curves developed by Brandt and Belton (1962) have been much used in neutral hydrogen work, as they may be inverted to give a mass distribution directly. The necessary functions are well tabulated (Brandt and Scheer, 1965). The Brandt curves are characterized by a maximum rotation velocity V_{max} at a radius R_{max}, also called the turn-over radius. There is also a shape parameter n, which gives more sharply peaked rotation curves for larger values of n. The general equation is

$$v(R) = \frac{V_{\max} \times R/R_{\max}}{[1/3 + 2/3(R/R_{\max})^n]^{3/2n}} \qquad (9)$$

The only physical feature of the Brandt curve is that, at large radii; the galaxy must appear as a point mass and the rotation velocity is then Keplerian. There is very little evidence from observations as to the nature of actual rotation curves beyond the turnover radius, but the Brandt curve is often a good fit up to this point, and the derived mass within this radius compares well with masses derived by fitting concentric spheroids. The total mass derived by extrapolating the observed rotation curve along the best-fitting Brandt curve is, however, much larger, and we have the rather unsatisfactory result that much of the mass of the galaxy lies beyond the observed region. Fitting a rotation curve model to a number of galaxies does offer a convenient and standard way of comparing the mass and derived quantities of these galaxies, but some care must be exercised in interpreting the results. The best procedure seems to be to quote a mass out to some standard radius such as the Holmberg (1958) radius. The angular momentum distribution may also be derived from the fitted density distribution, and this is of interest with respect to theories of galaxy formation from a condensing cloud of gas. The Brandt curve is characterized by only three parameters: R_{max}, V_{max}, and the shape parameter *n*. Since the angular momentum scales as $R_{max}^2 V_{max}^3$ and the mass as $R_{max} V_{max}^2$, we must avoid comparing any two parameters such as mass and angular momentum derived by fitting the Brandt curve, as they will then be mathematically correlated, independent of any real physical correlation between mass and angular momentum. Indeed, in the absence of real correlation between mass and angular momentum a graph of $R_{max}^2 V_{max}^3$ versus $R_{max} V_{max}^2$ has a slope determined by the relative dispersion in the distributions of R_{max} and V_{max}. Measurements of angular momentum are also rather unsatisfactory, as most of the angular momentum lies beyond the observed rotation curve.

For those 21-cm observations where there is insufficient angular resolution to measure the radius of maximum rotation velocity directly, a mass may still be obtained by estimating V_{max} from the width of the profile and R_{max} from the optical size of the galaxy. Figure 11.3(b) is a plot of R_{max} / a [where *a* is the Holmberg (1958) diameter] for 21 galaxies for which the rotation curves have been determined optically from long-slit spectroscopy of HII regions. The ratio is not a function of the morphological type, and the histogram is quite sharply peaked with $R_{max} \approx 0.1a$. If R_{max} cannot be measured, then we can estimate it as one-tenth *a* in order to obtain a mass estimate. For irregular galaxies a mass may be estimated from the virial theorem (e.g., Volders and Högbom, 1961); the mass will be

$$M = \frac{kaV_{\text{r.m.s.}}^2}{G} \qquad (10)$$

where *a* is the diameter of the galaxy, *G* is the gravitational constant, $V_{\text{r.m.s.}}$ is estimated from the width of the velocity profile, and *k* is a constant of order unity which depends upon an assumed model for the density and velocity distribution.

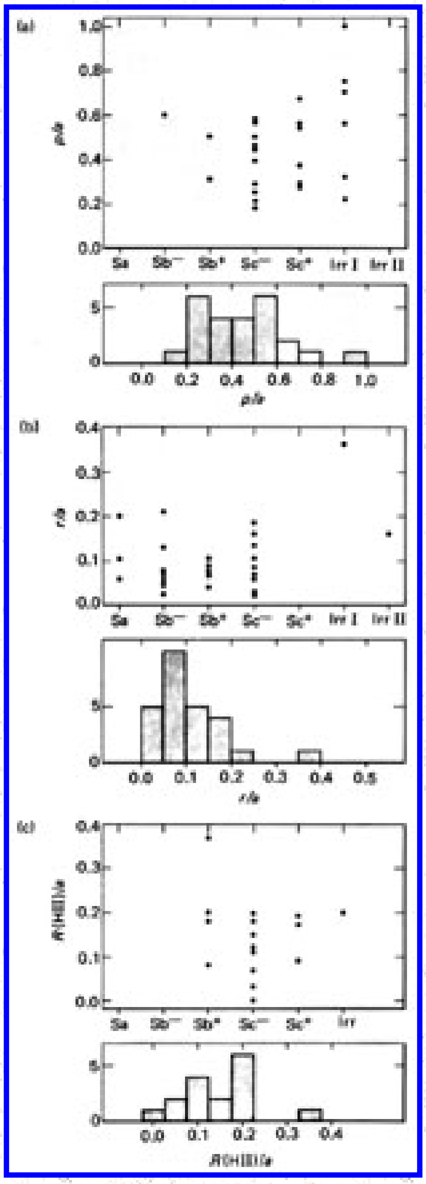

Figure 11.3. Plot against morphological type of galaxy and a histogram for (a) turnover radius, ρ/a, for galaxies observed by Rogstad, Rougoor, and Whiteoak (1967) (b) radius of maximum rotation velocity for optically derived rotation curves (c) radius of maximum HII region count, R(HII) / a, for galaxies observed by Paul Hodge. [M. C. H. Wright, Astrophys. J. (1971) 166:455.1

d) Noncircular Velocities

Noncircular velocities are apparent as departures of the isovelocity contours from symmetry about the major and minor axes. In particular we are interested in analyzing the isovelocity contours for expanding hydrogen and for streaming motions in the vicinity of spiral arms as predicted by the density wave theory (see Chapter 4 and also Lin, Yuan, and Shu, 1969). Analysis of these effects may be made by fitting the isovelocity contours with a model rotation curve, $V = V(r)$, and a set of parameters such as the systemic velocity, inclination, position angle, and rotation center.

The fitting for $V(r)$ can take place over the whole plane of the galaxy, with a higher weight given to points near the major axis. Having obtained the best-fit rotation curve, model isovelocity contours can then be subtracted from the observed isovelocity contours to give the residual velocity field. Examination of the residuals then shows, more clearly the systematic noncircular or "peculiar" velocities. It should be noted that the isovelocity contours and the residual velocity field are velocities weighted by the hydrogen distribution within the beam area, and particular care must be taken in interpreting the results. The effect of beam smoothing is to bias the measured velocity toward that of hydrogen concentrations within the beam. Two examples may be given

1. A galaxy which is a few beamwidths in diameter and which has a steep rotation curve toward the center has isovelocity contours drawn at intervals of the velocity resolution with a separation less than the observing beamwidth. Broad-frequency profiles will be observed, and the estimated rotation curve will have a smaller slope than the true curve.

2. Suppose that the hydrogen distribution has the form of spiral arms with separation rather less than the observing beamwidth. Observations between the spiral arms where there is not much HI will give a beam-smoothed profile with a velocity biased toward that of the nearest spiral arm. There is usually a gradient in the rotation velocity, and observations on the inner and outer edges of the spiral hydrogen concentration will yield velocities biased in opposite directions. We may be looking for just this sort of velocity, perturbation resulting from streaming motions near spiral arms! Clearly, caution must be exercised in drawing conclusions from observed peculiar velocities.

11.5. INTERFEROMETRIC OBSERVATIONS

11.5.1. Position Profiles

An interferometer with a multi-channel receiver is an inherently powerful tool for line observations, because the phase in each velocity channel contains information about the position of the source of radiation received in that velocity interval. A phase relationship over several channels can confirm a detection of a weak signal, while for stronger signals the phase gives the relative position in the sky of radiation received in each velocity channel. A plot of position versus velocity is often called a position profile.

11.5.2. Observations of External Galaxies

For a rotating galaxy, hydrogen radiating Galactic and Extra-Galactic Radio Astronomy at different velocities will arise from regions of the galaxy (such as those in Figure 11.2) delimited by the isovelocity contours. If observations are made with an interferometer whose baseline has an orientation close to the position angle of the major axis of the galaxy, and whose length, D, is not so great that the hydrogen distribution is appreciably resolved (i.e., $a > \lambda / D$, where a is the diameter of the galaxy), then the interferometer phase in each velocity channel indicates the distance along the major axis of hydrogen radiating in that velocity interval. The position profile is then a plot of the centroid positions of the regions in Figure 11.2 weighted by the hydrogen distribution (and smeared by random velocities, the observing beam, and the velocity filter). The amplitude in each velocity channel is roughly the product of the hydrogen density multiplied by the area of these regions. Observations of a number of galaxies have been made in this manner at the Owens Valley Radio Observatory (Rogstad, Rougoor, and Whiteoak, 1967). The amplitude-velocity and phase-velocity plots are a function of both the hydrogen distribution and the rotation curve, and the position profile obtained is subject to various interpretations.

11.5.3. Interpretation of the Data

a) Rotation Curves

For a solid-body rotation curve the iso-velocity contours are everywhere parallel to the minor axis, and the position profile along the major axis reproduces the shape of the beam-smoothed rotation curve. For any other rotation curve, interpretation is more difficult and we must resort to model fitting. If the rotation velocity falls to small values at a large radius, as in Figure 11.1, then the isovelocity contours form small closed areas at the high velocities, as in Figure 11.2. Provided that these closed regions occur well within the HI distribution, then the amplitude decreases at the velocity corresponding to the appearance of small closed regions in the isovelocity contours. The position indicated by the interferometer phase at this velocity gives an estimate of the "turnover radius," where rotation velocity is a maximum. This was the original interpretation given to the position profiles by Rogstad et al. (1967). Through a model-fitting procedure they deduced the turnover radius of the rotation curve and hence together with the rotation velocity the masses of the galaxies.

b) Hydrogen Distribution

The turnover radius deduced by Rogstad et al. (1967) is, on the average, a factor of two larger than rotation maxima measured by Burbidge, Burbidge, and Prendergast (1963), and others, by means of optical long-slit spectroscopy of HII regions.

This leads us to consider an alternative interpretation of the position profile in terms of the extent of the hydrogen distribution (Wright, 1971a). If the rotation velocity does not decrease beyond the maximum, as in Figure 11.1, but instead remains at a high value, then the small closed regions do not appear in the isovelocity contours. The amplitude response then decreases at a velocity where there is not much hydrogen. The position profile at this velocity then tells us the extent of the hydrogen distribution.

c) Shape of HI Distribution and Rotation Curve

In either of the above interpretations the position profile always gives us a lower limit to the extent of the hydrogen distribution, and comparison of this radius with that of the total mass and HII region distribution shows that the HI distribution is much wider than either (see Figure 11.3).

We can use the disagreement between the optically derived rotation maximum and that deduced from the first interpretation to invert the argument as follows: If the first explanation is not correct, then the rotation velocity cannot fall to a low value as in Figure 11.1, but must remain at a high velocity within the extent of the hydrogen distribution. This is quite consistent with observed rotation curves (see Section 11.7), which are indeed rather flat-topped.

11.6. APERTURE SYNTHESIS OBSERVATIONS

11.6.1. Observational Requirements

a) Angular Resolution

Model fitting of low-resolution maps or of simple interferometer observations is clearly inadequate to analyze the details of the HI distribution and kinematics in spiral galaxies. Aspects concerning the spiral structure can be investigated only when we have obtained a map of the neutral hydrogen distribution with a resolution comparable to the angular separation of the luminous spiral arms. In the nearest galaxies this is of the order of 1 minute arc, and such resolution can at present be obtained only by the use of aperture synthesis techniques. Aperture synthesis observations of external galaxies are currently being made at four observatories. The instruments being used are the Cambridge Half-Mile Telescope in England (Baldwin et al.; 1971), the 12-element Westerbork Synthesis Radio Telescope (Brouw, 1971) in the Netherlands, the 2-element interferometer at the Owens Valley Radio Observatory, and the 3-element interferometer at the National Radio Astronomy Observatory (NRAO) in the United States.

Observations are usually made with the telescopes at each of several separations at which the telescopes track the source over a range of hour angle. Maps of the sky brightness are computed from a Fourier inversion of the recorded data. This is the method of Earth rotation synthesis (see Chapter 10). The maximum angular resolution is determined by the largest interferometer baseline, D, used in the aperture synthesis. The synthesized beam subtends a solid angle $(\lambda / D)^2$ cosecδ, where δ is the declination of the source.

If observations are made with interferometer baselines at intervals d to a maximum D, then a grating sidelobe response occurs at an angle λ / d in RA and $(\lambda / d) \times$ cosec δ in declination. The area of sky which can be mapped without ambiguity from grating side-lobes is $(\lambda / d)^2$ cosec δ. The baseline interval, d, should be sufficiently small that this area includes the extent of the neutral hydrogen radiating in any velocity channel; otherwise the synthesized map will be confused by grating sidelobes. There is no point, however, in making d much smaller than the diameter of the antennas, since the reception pattern of these then limits the area of sky which can be mapped.

b) Frequency Resolution

Observations of spiral galaxies show that the greatest range of velocities expected is about ± 300 km sec^{-1}, and it is desirable that a multi-channel receiver should cover the whole of this range. The maximum useful resolution in velocity is dependent on the angular size of the synthesized beam, since in general the line-of-sight radial velocity varies in a systematic way across the galaxy. Near the center of the galaxy the area of the synthesized beam intersects many isovelocity contours (see Figure 11.2); a large range of velocities is present within one beam area, and a high-velocity resolution is not required. Further out in the galaxy, however, there is a small range of rotation velocities within one beam area and a higher resolution might be useful. Dispersion in the gas along the line of sight might be of order 10 km sec^{-1} and this accordingly is a useful resolution. Thus a desirable minimum for a multi-channel receiver is 60 channels, each 10 km sec^{-1} wide, for each interferometer.

c) Sensitivity

Suppose that we spend equal times observing at each interferometer baseline at intervals d to a maximum D. The total integration time is proportional to D / d. The angular resolution obtained is proportional to $\theta = \lambda / D$ so that for a given stepping interval d (which is determined by the angular extent of the hydrogen) the fluctuations in aerial temperature, T_a, are proportional to $\theta^{1/2}$. As a result of the aperture synthesis, only flux collected by the *synthesized* beam contributes to the effective aerial temperature of the source. The aerial temperature, T_a, due to a source of uniform brightness temperature, T_b, is obtained by multiplying T_b by the ratio of the synthesized beam area to the antenna beam area. Thus $T_a \propto T_b \theta^2$, and the sensitivity of the telescope to extended objects *decreases* with resolution as

$$T_a / \Delta T_a \propto T_b \theta^{3/2} \qquad (11)$$

This degrading of the signal-to-noise ratio with increasing resolution can be offset by spending a longer time at the larger aerial spacing, and the reason for this requirement may be understood in terms of the increased rate of sampling of the (u - v) plane at the longer baselines (see Chapter 10). It does, however, mean that the sensitivity requirements may limit the resolution rather than the available baseline.

11.6.2. Correlation Receivers

The requirement for a large number of velocity channels has favored the use of cross-correlation receivers. The principle on which the cross-correlation receiver operates is that, for two random time-varying signals, $V_1(t)$ and $V_2(t)$, the cross-correlation function

$$\sigma(\tau) = \int V_1(t) V_2(t - \tau)\, dt \qquad (12)$$

is the Fourier transform of the visibility spectrum $V_1(\omega)$ $V_2(\omega)$ of the two signals. Here the signals $V_1(t)$ and $V_2(t)$ are the voltages from the two telescopes forming the interferometer, and $V_1(\omega)$ $V_2(\omega)$ is the cross-correlated spectrum at an angular frequency ω. The cross-correlation function is sampled over a range of delays ± ΔT, ± 2ΔT, . . . to a maximum delay ± T sec, and the visibility spectrum is obtained as the Fourier transform of the sampled cross-correlation function.

The maximum delay T determines the resolution of the synthesized frequency channel, 1/2T Hz, and the sampling interval AT produces a grating response in frequency at an interval 1/2ΔT. The exact shape of the equivalent frequency filter is the Fourier transform of the weighting applied to the cross-correlation function. If the latter is transformed with equal weight applied to each delay, then the equivalent frequency filters have a (sinθ) / θ response, with a half-width of 1.2 / 2T Hz and 22% sidelobes. Both positive and negative delays must be sampled to determine the amplitude and phase of the interferometer, and the correlation receiver is equivalent to a bank of T / ΔT adjacent frequency filters at intervals of 1 / T Hz.

The cross-correlation may be achieved in practice either in an analogue device using physical delay steps or in a digital correlator. In the latter, simplified logic results if one-bit sampling of the correlation function is employed (so that only the sign of the sampled correlation function is recorded). This results in some loss in signal-to-noise ratio, but the visibility spectrum may be fully restored (Weinreb, 1963) through the Van Flyck correction. While increasing the complexity of the data processing, as an extra Fourier transform must be computed, the correlation receiver has a number of advantages over a conventional filter bank receiver in that the relative sensitivity of the frequency channels is easily calibrated. A digital correlator has good stability essential for a good synthesis, and the additional advantage that the bandwidth can be changed by simply changing the clock rate which determines the sampling interval.

11.6.3. Data Reduction

a) Frequency Fourier Transform

If a correlation receiver has been used, then the first stage is a Fourier transform to recover the visibility spectrum of the signal. It should be noted that the shape of the frequency, filters is under our control as we can apply a weighting function to the correlation function before computing the Fourier transform (this is equivalent to convolving the spectrum after the Fourier transform). Thus we can reduce the 22% frequency sidelobes associated with a uniform weighting function, at the expense of an increased half-width. The frequency Fourier transform is often made in an on-line computer, which receives data directly from the correlator.

b) Calibrations

There are two basic calibrations in addition to the usual interferometer baseline and system gain-and-phase calibrations of a broad-band interferometer (see Chapter 10). These are

1. to determine the relative sensitivities of the frequency channels

2. to determine the sensitivity and system phase of the telescope as a function of frequency.

c) Spatial Fourier Transform

Each frequency channel may be separately Fourier inverted as for a broad-band interferometer, as discussed in Chapter 10. The chief problem is the large quantity of data to be processed, and the computation may take several hours - even on the largest computers using fast Fourier transform techniques.

d) Presentation of the Data

The end-product of the above processing is a series of maps of the hydrogen distribution in the different frequency channels. These maps form the basic data, which can be considered as a three-dimensional array with *x*, *y*, and frequency coordinates. The maps of frequency channels containing line emission may be combined to produce a map of the integrated line emission and a map of frequency spectra at a grid of points on the area of sky studied. A velocity (or profile width) can then be fitted to the frequency spectra and a map of isovelocity contours drawn across the source. There is obviously a considerable data-handling problem associated with mapping a 1° square of sky, say, with an angular resolution of 1 minute arc at 60 different velocities, and the basic problem is presenting the information in a digestible form. It is to be expected that fairly exotic techniques will eventually be used in this final and most important stage of data reduction, namely, in the interface between the data and the astronomer.

11.7. HIGH-RESOLUTION MAPS

7.1. Observations of M33 with the Cambridge Half-Mile Telescope

a) Observations

The highest resolution observations of an external galaxy so far made using aperture synthesis techniques are those of M33, made with the Cambridge Half-Mile Telescope (Wright, Warner, and Baldwin, 1972). This telescope consists of two 9-m paraboloids on an east-west baseline and was designed as an aperture synthesis instrument for observing extended objects. The observations of M33 have an angular resolution of 1.5 minutes are in RA and 3 minutes arc in declination, equivalent to a 300 × 600 pc area at the distance of M33 (690 kpc). (This compares with a linear resolution of 210 pc in the

Magellanic Clouds using the Parkes 210-foot telescope.) The velocity resolution of these data is 39 km sec^{-1}, commensurate with the range of velocities expected within a 300 × 600 pc area over most of the galaxy. Observations were made at 59 interferometer baselines with telescope separations at 6m intervals to a maximum of 360m. The full baseline (720 m, ≈ a half-mile) was not used for reasons of sensitivity, as discussed in the previous section. The data were obtained using an analogue cross-correlation receiver and were processed much as described in the previous section. The basic data are in the form of nine maps of the HI distribution at 26 km sec^{-1} intervals. These nine maps cover the range of velocities found in the neutral hydrogen of M33.

b) Integrated HI Brightness Distribution

For these observations the half-width of a velocity channel is larger than the velocity interval between the channels, and a simple addition of these nine maps suffices to construct a map of the integrated hydrogen distribution in M33 (Figure 11.4). This map is of the surface brightness temperature of the hydrogen line integrated over the line profile.

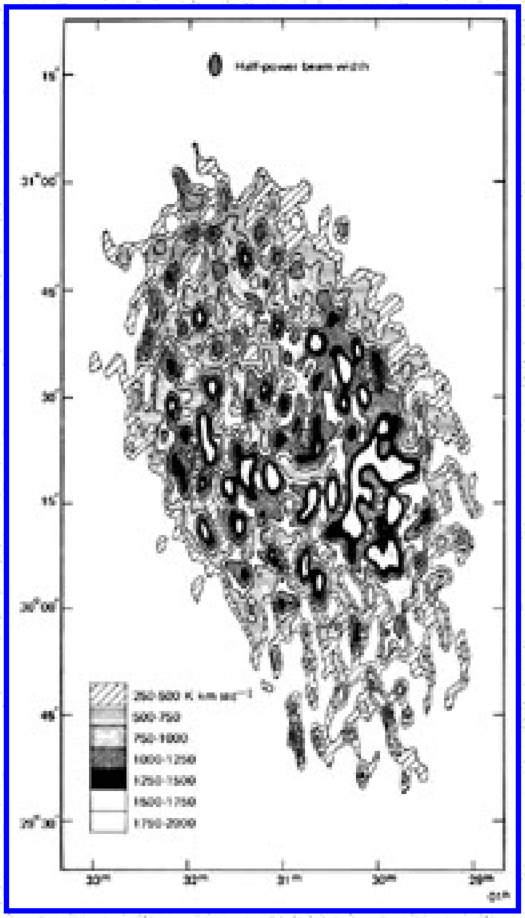

Figure 11.4. Integrated HI brightness in M33 to an angular resolution of 1.5 × 3 minutes arc. [Wright et al., Monthly Notices Roy. Astron. Soc. (1972) 155:337.]

If the galaxy is everywhere optically thin to the line radiation, then the map also represents the distribution of the HI surface density projected along the line of sight. The peak brightness temperature observed is 50° K but the distribution is in places unresolved in both angle and velocity so that the true brightness temperature may exceed 100° K and the line radiation may not be optically thin. Where the radiation is not optically thin, the brightness temperature gives only a lower limit to the surface density. There is no direct evidence of optically thick HI from absorption of continuum sources lying behind or in the disk of M33, and we can adopt as a working hypothesis that the line radiation is optically thin, so that the map of the integrated brightness temperature is also a map of the HI surface density.

c) Large-Scale Structure

The large-scale structure of the hydrogen distribution may be obtained with a higher signal-to-noise ratio on a lower-resolution map (which may be obtained in aperture synthesis observations by simply not including data from the larger interferometer spacings in the Fourier transform). A low-resolution map generated from the above data agrees well with the map obtained by Gordon (1971) with the NRAO 300-foot telescope and described in Section 11.4. Figure 11.5 is an integration in elliptical rings (circular in the galaxy plane) of the brightness temperatures of Figure 11.4, and shows that the average radial distribution is a plateau with a very sharp cut-off at the edges. The radial distribution in Figure 11.5 is not in good agreement with the suggestion by Roberts (1967) that the HI has a ring distribution as in M31. The average projected surface density is $\approx 3 \times 10^{21}$ atoms cm^{-2}, or 1.7×10^{21} cm^{-2} viewed normal to the plane of the galaxy. The sharp fall in density at the edges of the galaxy could be due to ionization by an inter-galactic flux of UV photons, as discussed by Sunyaev (1969). An alternative explanation is that the sharp gradients at the edges of the galaxy are associated with the warping of the plane of the HI disk indicated by the wings of the galaxy. A hat-brim model is envisaged with an increasing inclination of the plane of the galaxy to the line of sight along the edges of the galaxy at the ends of the minor axis.

There is a marked asymmetry in the HI distribution with a massive HI complex in the south-preceding quadrant of the galaxy.

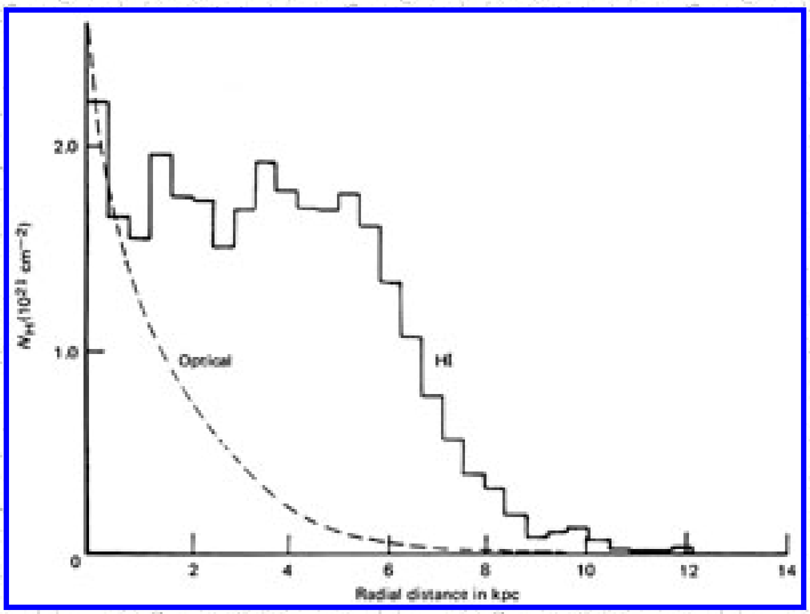

Figure 11.5. Integration in circular rings in the plane of M33 of the integrated brightness distribution. [Wright et al., Monthly Notices Roy. Astron. Soc. (1972) 155:337.]

d) Small-Scale Structure

The HI distribution is broken up into a large number of concentrations only partially resolved by the 1.5 × 3.0 minute arc beam. These concentrations have a typical peak surface density of 2.7 × 10^{21} cm^{-2} and a space density of ~ 1 to 2 atom cm^{-3}. They perhaps resemble the complexes discussed by McGee (1964) in the spiral arms of our galaxy, having sizes ≈ 500 to 2500 pc and densities ≈ 0.5 cm^{-3}, and those in the Large Magellanic Cloud having mean diameter 600 pc and density ≈ 1 cm^{-3}. A spiral arm structure can be seen in the inner regions of the galaxy and is most evident in the trough running south from the galactic center (Figure 11.4). A best-fitting logarithmic spiral structure agrees with the optical spiral arms and the measured ratio of the average projected HI density in the arm and interarm regions is between 2 or 3 to 1. The troughs between HI concentrations are barely resolved by the beam, and the true density ratio may be as large as 6 to 1. An infinite contrast ratio is, however, ruled out by these observations.

e) Comparison with Optical Features

The extent of the HI distribution corresponds well with that of a well-exposed blue-print of the galaxy and the major and minor axis widths are close to the 83 × 53 minute arc given for the optical size by Holmberg (1958).

Figure 11.6 shows a superposition of the HI peaks onto a plate taken through a narrow-band red filter. It can be seen that the Mapping Neutral Hydrogen in External Galaxies HI concentrations follow the line of the optical spiral arms well in the south of the galaxy. The correlation is not so clear, and there are no strong HI concentrations on the northern spiral arm between the nucleus and NGC 604, where there is again a large concentration of HI. The contrast of the spiral arms is better in the composite HI + HII distribution in Figure 11.6 than in either the HI or HII regions separately, which indicates that the HI and HII are in some sense complementary.

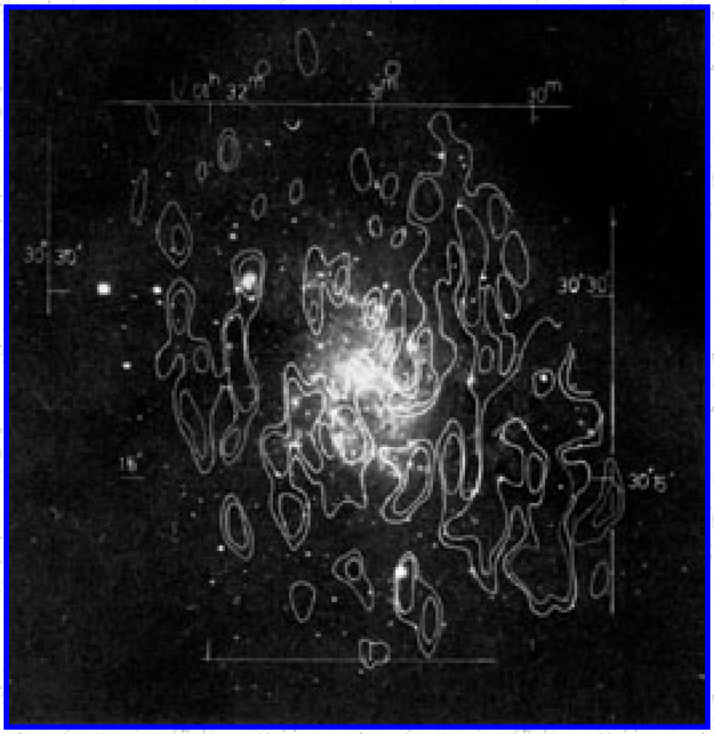

Figure 11.6. Superposition of the peaks of the HI distribution of M33 on a red print showing mainly HII regions.

f) Rotation Curve and Total Mass

The isovelocity contours (Figure 11.7) conform well to the pattern expected for a rotating galaxy and the rotation curve measured along the major axis is shown in Figure 11.8. The total mass can be derived by fitting a model rotation curve. The observed rotation curve has been fitted to three different types of rotation curve: a Brandt rotation curve with $n = 1.0$, a curve corresponding to an exponential distribution of mass (as discussed by Freeman, 1970), and an eighth-order polynomial. In all three cases the fitted curves agree with the observed rotation curve within 3 km sec^{-1}, and it will clearly be difficult to distinguish among them. The distributions of mass with radius deduced from these three fitted rotation curves are very similar within ≈ 20 minutes arc radius but diverge outside this radius. Using a Brandt curve with R_{max} = 30 minutes arc, V_{max} = 100 km sec^{-1}, and $n = 1.0$ gives a mass within 45 minutes arc of 1.7×10^{10} $M_{\odot}$. The HI content is then some 9%, typical for an Sc galaxy. Because of the very flat rotation curve, the total mass of the galaxy extrapolated beyond the observed rotation curve is some 5×10^{10} $M_{\odot}$), but this does not have much meaning.

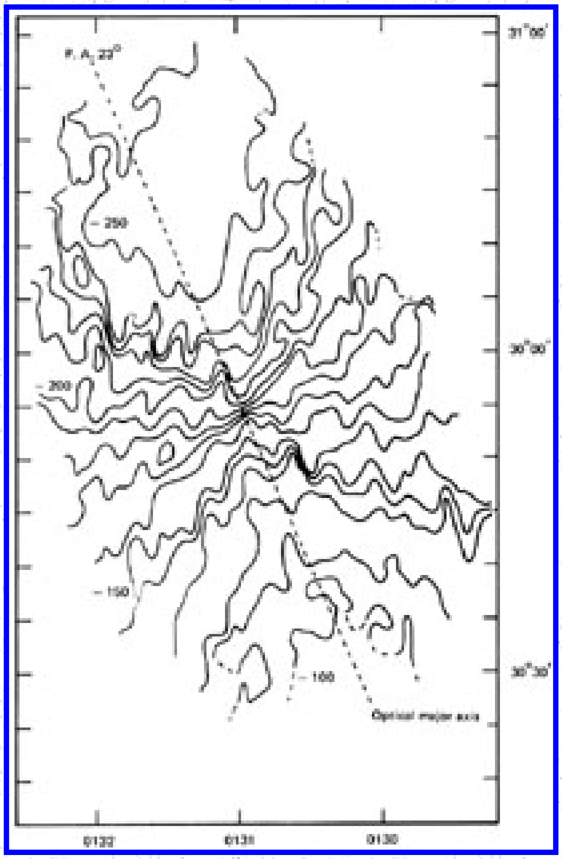

Figure 11.7. Isovelocity contours in M33 drawn at intervals of 10 km sec^{-1}.

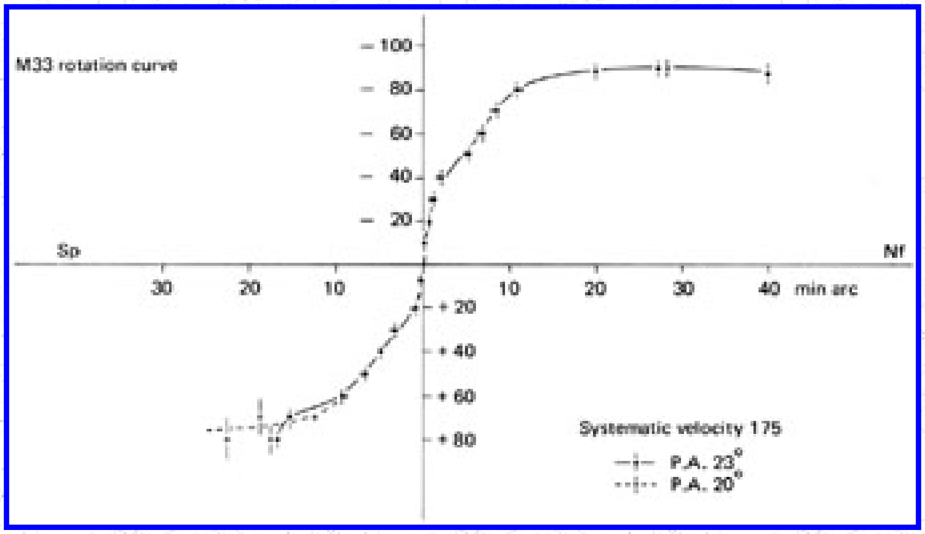

Figure 11.8. Rotation curve measured along the major axis of M33. The rotation velocities uncorrected for inclination are referred to a heliocentric systematic velocity of -175 km sec^{-1}.

g) Peculiar Velocities and Streaming Motions

It is clear from Figure 11.7 that there are local departures of the isovelocities from circular motion which exceed the noise level. It is essential, however, to consider the effect of beam averaging. A superposition of Figure 11.4 and Figure 11.7 shows that the deformations in the isovelocity contours often correspond to their crossing between HI peaks. The velocity in the interarm region is a beam average of the velocities of all HI concentrations within the beam at that time, and we may consequently discount many of the departures from smooth isovelocities. Some of the departures are real, however, and local peculiar velocities can be 20 to 30 km sec^{-1}.

The line-of-sight velocity due to the rotation of the galaxy may be computed by selecting values for the rotation center, position angle, inclination, and rotation curve of the galaxy. If this model velocity field is subtracted from the observed velocity field, errors in the parameters selected show up in the residual velocity field with characteristic symmetries and enable best values for the rotation parameters to be determined. The residual velocity field may then be examined for systematic streaming motions predicted by the density wave theory of spiral arms. From the present observations of M33 it appears that such streaming motions are less than about 5 km sec^{-1}.

h) Comparison of Neutral and Ionized Hydrogen Velocities

In Figure 11.9 are plotted the velocities of the large HII regions measured by Mayall and Aller (1942) against the HI velocity at the HII region position. Because of the relatively large beamwidth (1.5 × 3 minutes arc), the HI Velocities are best regarded as an average velocity of HI in the vicinity of the HII region. The HII region velocities are local velocities of ionized gas within the HII region. The straight line has a slope of 1, showing that there is no systematic difference between the velocities of neutral and ionized gas. The vertical scatter in Figure 11.9 shows that, the velocity of an HII region can differ by 20 to 30 km sec^{-1} from that of the neutral gas. Indeed, measurements within a single HII region can differ by the same magnitude. Estimates of the mass of gas in large HII regions, e.g., in 30 Doradus in the LMC (Faulkner, 1967) and in NGC 604 in M33 (Wright, 1971b), show that velocity dispersions of this magnitude will disperse the HII region in $\approx 10^7$ years.

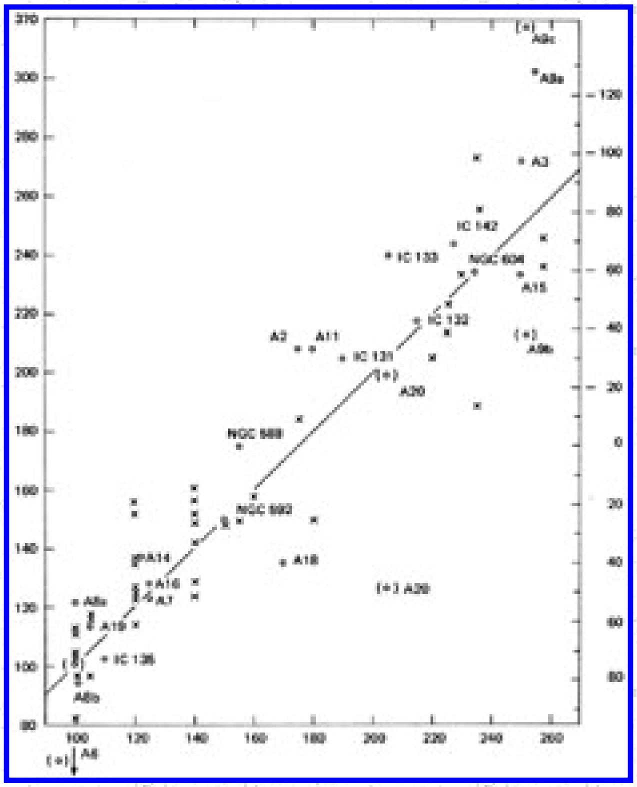

Figure 11.9. Velocities of HII regions (ordinate) plotted against the neutral hydrogen velocity at the position of the HII region. Open circles, *o*, are HII regions measured by Mayall and Aller (1942) with velocities by Brandt (1965); (*o*) velocities are measured by Mayall and Aller; (*x*) velocities are measured by Carranza et al. (1968). The left ordinate and abscissa scale are heliocentric, and the right ordinate is with respect to a systematic velocity of -175 km sec^{-1}. The line has a slope of 1.

11.7.2. Observations at the Owens Valley Radio Observatory

a) Observations

The two-element interferometer at the Owens Valley Radio Observatory has been used to map a number of late-type galaxies to an angular resolution of 2 minutes are and a velocity resolution of 21 km sec^{-1}. The Owens Valley interferometer is able to track sources over only a limited hour angle range but both E-W and N-S spacings are available so that good coverage of the (*u* - *v*) plane can still be obtained. Fixed observing stations are positioned at 100-foot intervals, giving a grating sidelobe response at 20 minutes arc radius and enabling sources smaller than this to be mapped without confusion.

For larger galaxies special techniques must be used to eliminate the sidelobe response. A powerful technique, first used in the case of M101 (Rogstad and Shostak, 1971), is to iteratively subtract the synthesized beam together with its sidelobes from the maximum of the source region of the synthesized map. The iteration stops when the sources being subtracted are a small percentage of the original maximum or when the residual map approaches the noise level. A map, corrected for the sidelobe response, is then reconstituted by convolving the subtracted sources with a clean sidelobe-free beam and adding them back into the residual map.

This procedure may not result in a unique map, but there are some tests on the validity of the procedure, which is discussed in more detail in Chapter 10.

b) Integrated Hydrogen Distribution of M101

Figure 11.10 shows the integrated HI brightness of M 101 observed with a 4-minute-arc beam. Most remarkable in Figure 11.10 is the ring distribution and the marked asymmetry in the hydrogen distribution. If the gas is assumed to be optically thin, then the contour interval corresponds to an HI surface density of 1.4 atom cm^{-2}. For an assumed distance of 6.9 Mpc the integrated HI mass is 9×10^9 $M_\odot$. If the HI distribution is really symmetric and the asymmetry in the integrated brightness is due to variations in the spin temperature of the gas, then this mass would be increased by ≈ 25%. Assuming that the gas is optically thin, the central depression in the integrated brightness represents a surface density of ~ 3.5×10^{20} atom cm^{-2}. Monnet (1971) has observed a weak background of Hα radiation in several galaxies. In M101 the estimated plasma density is nearly. sufficient to account for the missing hydrogen, suggesting that the gas is highly ionized.

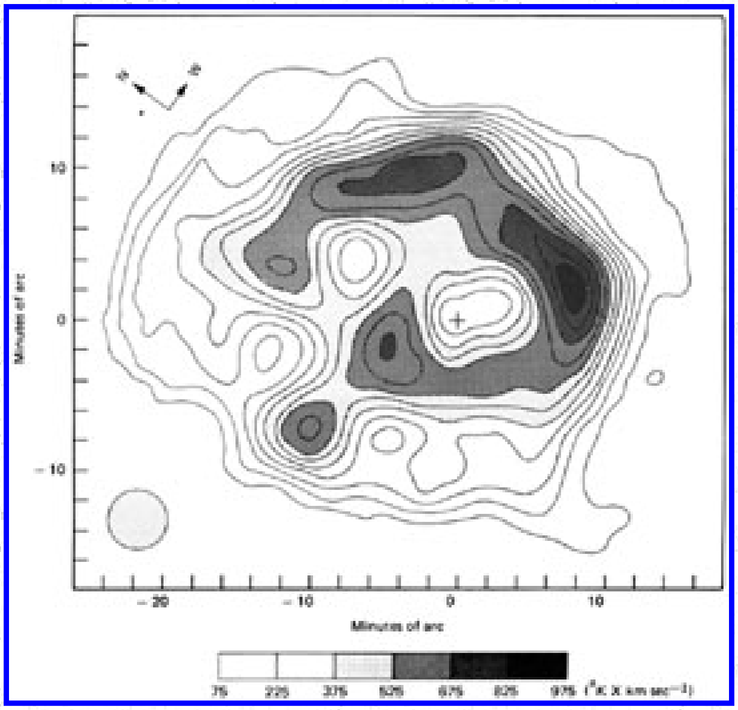

Figure 11.10. Integrated HI brightness in M101 to an angular resolution of 4 minutes arc.

c) Velocity Field and Streaming Motions in M101

The velocity field of M101 (Figure 11.11) derived from the HI observations (Rogstad and Shostak, 1971) displays many deviations of 10 ~ 20 km sec^{-1} from circular rotation of the gas. Many of these deviations are in the form of ridges in the vicinity of the luminous spiral arms. Rogstad (1971) has interpreted this as evidence for the density wave theory of spiral structure (see Chapter 4).

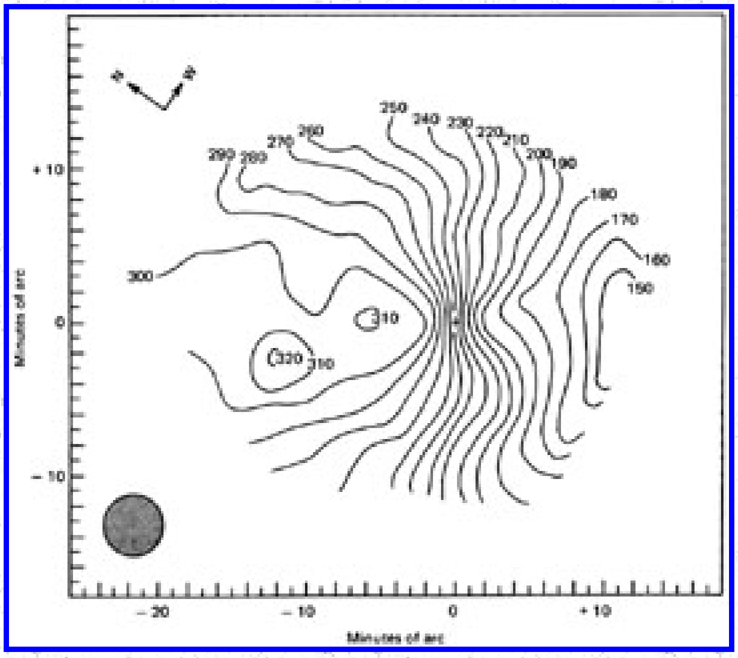

Figure 11.11. Isovelocity contours in M101.

There are further deviations in the isovelocity contours near the nucleus of M101 which could indicate expansion motions ≈ 40 km sec^{-1} in the vicinity of an inner spiral arm and coincident with a central nonthermal radio source. The outflow of HI is sufficient to account for the even deeper hole in the HI distribution of the nuclear region.

11.7.3. Comparison of the HI Distributions of Late-Type Galaxies

a) Observations

Several other galaxies have recently been mapped at the Owens Valley. NGC 6946 and IC 342 (Rogstad et al.,1973) ; NGC 2403, NGC 4236, (Shostak and Rogstad, 1973), and IC 10 (Shostak, 1974); M51, M81, and M82 (Weliachew and Gottesman, 1973); and Mafei 2 (Wright and Seielstad, 1973); IC 2574, and NGC 7640 (Seielstad and Wright, 1973). These observations have an angular resolution of 2 minutes arc and a velocity resolution of 10 or 21 km sec^{-1}.

NGC 2403 is an Sc$^-$ (Holmberg system) galaxy and is very similar in morphological form and stellar content to M33 [see the *Hubble Atlas of Galaxies* (Sandage, 1961)]. The integrated brightness distribution has a marked depression in the central region, similar to that in M101 but quite different from the HI distribution in M33. The three highest peaks in the integrated HI brightness distribution do not correspond well with the luminous spiral features, but rather lie in the dust lanes between the luminous spiral arms. A number of bright HII regions can be seen around the edges of these HI peaks. This can also be seen in places in M33. The rotation curve, as in M33, is very steep at the center and has a large constant-velocity region extending to the boundary of the detected hydrogen (as suggested in Section 11.5).

NGC 4236 is classified Sc$^+$ by Holmberg (1958) and SB 7 by de Vaucouleurs (1964). A number of hydrogen concentrations are found, the largest peak in the north corresponding to a bright HII complex at the end of the "bar." The HII regions in the south, on the other hand, tend to lie around the HI peaks. All the rotation curves of NGC 4236, NGC 2403, and M33 have the same characteristic shape if scaled to common rotation curve maxima, R_{max} and V_{max},

IC 10 is an irregular galaxy in a heavily obscured region of the sky. The integrated HI distribution shows a number of peaks and a large depression where the integrated brightness falls to zero. The peak brightnesses of all three galaxies are very similar ($\approx$ 1200°K km sec^{-1}), although the inclinations are different.

b) Five Scd Galaxies

In a comparison of the five Scd galaxies, M33, NGC 2403, IC 342, M101, and NGC 6946, Rogstad and Shostak (1972) find sub stantial similarities in the hydrogen distributions and rotation curves. The integral HI parameters are nearly constant or scale with the Holmberg (1958) diameter. Eighty percent of the observed HI mass lies within the Holmberg diameter for each galaxy. The mean hydrogen content is 11% of the total mass within this same boundary, and the central HI surface density is also nearly constant ($\simeq 8 \times 10^{20}$ atom cm^{-2}).

All the rotation curves are observed to be flat-topped, with a maximum velocity proportional to the Holmberg diameter. Because of the flat-topped rotation curves, the total masses extrapolated to infinite radius are indeterminate, but the total mass within the Holmberg radius is proportional to $R_{H_0}{}^3 \; V_{\mathrm{max}}{}^2$, and therefore scales as $R_{H_0}{}^3$ for these five galaxies. The constancy of the integral properties within one morphological class is an important justification for the use of the morphological classification system for spiral galaxies.

11.7.4. Central Hydrogen Depressions

As suggested by Roberts (1967) (see Section 11.4.5), it appears that a central depression in the HI surface brightness is a common feature in late-type spiral galaxies. M31 is the most obvious case where an HI "ring" is a good overall description. For the other galaxies so far observed the HI distribution is better described in terms of an asymmetry and a central depression. In no observed galaxy does the surface brightness resemble the overall light distribution, which is exponentially decreasing, or the total mass distribution (deduced from rotation curves or from an assumed mass-to-light ratio). The total mass and light distribution are centrally peaked; the HI surface brightness is rather flat or centrally depressed. There are several possible explanations:

1. The usual assumption that the gas is everywhere optically thin may not be correct. It is almost certainly true that small cold optically thick clouds occur locally in every galaxy. If the spin temperature or the cloudiness of the HI varies systematically across the galaxy, then the surface brightness of HI line radiation may not resemble the HI surface density distribution. This explanation requires lower spin temperatures or very clumpy HI in the central regions of galaxies.

2. The thickness of the HI layer may increase with radius, as observed in our galaxy (Kerr and Westerhout, 1965). The HI layer thickness in M33 can be estimated from the measured velocity dispersion in the HI line profiles. If we assume that the vertical velocity dispersion (c^2) supports the gas against gravitational attraction, then the half-thickness ($\bar{z}$) of the gas layer is given by Mestel (1963) as

$$\bar{z} = \frac{c^2}{2\pi G\sigma} \tag{13}$$

   where σ is the total mass surface density in the plane of the galaxy. σ has been estimated from a mass-model fitted to the rotation curve and decreases with radius. To first order the observed velocity dispersion in M33 is constant; therefore the HI layer thickness increases with radius. In M33 the HI surface density is roughly constant with the radius (see Figure 11.5) ; therefore the HI volume density decreases with radius. This is consistent with the observed decrease in the rate of star formation with radius in M33 (Madore et al., 1973). In M31 a ten-fold increase in layer thickness would make the HI volume density in the central regions equal to that at the position of the ring.

3. The gas in the central regions may be ionized. Monnet (1971) has observed a weak background of Ha radiation in the central regions of several galaxies. In the case of M31, however, the emission measure was less than 10 cm^{-6} pc, which is too small by an order of magnitude to give a surface density comparable with that of the HI peak.

4. The gas could be in molecular form without any observable consequences. Molecular hydrogen has been seen in the far-ultraviolet absorption spectra of the star ξ Persei, which has a strong ultraviolet continuum emission (Carruthers, 1970). However, observation of H_2 in external

galaxies is far beyond present techniques.

5. Neutral hydrogen is expanding away from the central regions of the Milky Way (see Oort, 1964; Kerr, 1967). The 3-kpc-arm feature of our galaxy is expanding at a velocity of some 53 km sec^{-1}, while asymmetry in the rotation curve for our galaxy can be interpreted as a 7 km sec^{-1} expansion in the vicinity of the Sun. The outflow of neutral gas from the central regions (about $1 M_{\odot}$ per year) might be partially balanced by an inflow (under one interpretation of the high-velocity gas seen at high latitudes in the galaxy; see Oort, 1967), but is otherwise sufficient to deplete the central regions of HI in some 10^7 to 10^8 years.

   Expansion motions have been observed in the central regions of some external galaxies (e.g., M101) but in M31 they are less than 10 km sec^{-1} (Gottesman and Davies, 1970) and are too small to have removed a significant mass of HI away from the central regions.

6. The gas in the central regions may have been used up by star formation. Star formation would initially be fastest in the central regions of galaxies where the gas density is highest. At the present epoch the rate of star formation in M31 is at its peak in the region of the ridge at 10-kpc radius.

The correct explanation of the deficit of HI in the central regions is probably a combination of explanations (2) and (6), although in some instances explanations (3) and (5) may be highly significant. Explanations (1) and (4) are unknown factors.

11.7.5. Rate of Star Formation

The rate of star formation is presumed to depend on the gas density. Attempts to find a relationship of the form

$$\frac{d\rho_*}{dt} = \text{constant} \times \rho_g^n \qquad (14)$$

[where ρ_* is the star (or HII region), and ρ_g the gas density] have yielded different values for the exponent n. Comparisons of HII region and bright star counts with HI surface densities have been made for the SMC, M31, and M33. For bright stars in the SMC Sanduleak (1969) obtained a value of $n = 1.84 \pm 0.14$. In M31 Hartwick (1971) obtained a value of $n = 3.50 \pm 0.12$ by comparing HII region counts with Robert's (1966) HI density.

A comparison of the HI surface density in M33 (Wright et al., 1972) with HII region and star counts in M33 (Madore, 1971) finds a value of $n = 1.72 \pm 0.01$ for stars and $n = 3.15 \pm 0.18$ for HII regions. Most of the stars counted in M33 are the less massive O and B stars, whilst only large HII regions (excited by massive O stars) are included. The different values of *n* obtained in M33 tend to support the suggestion by Schmidt (1963) that *n* is the largest for the most massive stars. The values of *n* obtained for HII regions are in good agreement in M31 and M33.

11.8. CONCLUSIONS

The observations presented in the previous section represent the present state of the art of mapping neutral hydrogen in external galaxies. Aperture synthesis observations of a number of nearby late-type spiral galaxies are in progress at the present time, and we should soon be able to see if the HI distributions of, say, Sb and Sc galaxies are characteristically different.

Maps made with the Westerbork telescope to an angular resolution of 23 seconds arc should soon be available, allowing a detailed comparison of HI structure in many more galaxies. Details of the HI density and velocity distribution in the luminous spiral arms should make possible a much better understanding of star formation and of the dynamics of the spiral patterns.

REFERENCES

1. Avner, E. S., and 1. R. King. 1967. *Astron. J.* 72:650.
2. Baldwin, J. E., C. Field, P. J. Warner, and M. C. H. Wright. 1971. *Monthly Notices Roy. Astron. Soc.* 154:445.
3. Bergh, S. van den. 1960a. *Astrophys. J.* 131:215.
4. Bergh, S. van den. 1960b. *Astrophys. J.* 131:558.
5. Bottinelli, L. 1971. *Astron. Astrophys.* 10:437.
6. Bottinelli, L. Gougenheim, J. Heidmann, and N. Heidmann. 1968. *Ann. Astrophys.* 31:205.
7. Bottinelli, L. Gougenheim, and J. Heidmann. 1973. *Astron. Astrophys.* 25:451.
8. Brandt, J. C. 1965. *Monthly Notices Roy. Astron. Soc.* 129:309.
9. Brandt, J. C. and J. J. Belton. 1962. *Astrophys. J.* 136:352.
10. Brandt, J. C. and L. S. Scheer. 1965. *Astrophys. J.* 70:471.
11. Brouw, W. N. 1971. *Data Processing for the Westerbork Synthesis Radio Telescope.* Dissertation, Leiden University.
12. Burbidge, E. M., G. R. Burbidge, and K. H. Prendergast. 1963. *Astrophys. J.* 138:375.
13. Burke, B. F. 1967. *I. A. U. Symposium No. 31, Paper 31*. New York: Academic Press.
14. Cameron, M. J. 1971. *Monthly Notices Roy. Astron. Soc.* 152:403.
15. Carruthers, G. R. 1970. *Astrophys. J.* 161:L81.
16. Chandrasekhar, S. 1942. *Principles of Stellar Dynamics.* Chicago: University of Chicago Press.
17. Epstein, E. E. 1964. *Astrophys. J.* 69:521.
18. Faulkner, D. J. 1967. *Monthly Notices Roy. Astron. Soc.* 135:401.
19. Freeman, K. C. 1970. *Astrophys. J.* 160:811.
20. Gordon, K. J. 1971. *Astrophys. J.* 169:235.

21. Gottesman, S. T., and R. D. Davies. 1970. *Monthly Notices Roy. Astron. Soc.* 149:262.
22. Hartwick, F. D. A. 1971. *Astrophys. J.* 163:431.
23. Henize, K. G. 1956. *Astrophys. J., Supp. Ser.* 2:315.
24. Hindman, J. V. 1967. *Australian J. Phys.* 20:147.
25. Hindman, J. V., F. J. Kerr, and R. X. McGee. 1963. *Australian J. Phys.* 16:570.
26. Hodge, P. W. 1967. *Astron. J.* 72:129.
27. Hodge, P. W. 1969. *Astrophys. J.* 155:417.
28. Holmberg, E. 1958. Medd. Lunds, Ser. 2, No. 136.
29. Kerr, F. J. 1967. *I. A. U. Symposium No. 31*. New York: Academic Press.
30. Kerr, F. J. 1968. In *Stars and Stellar Systems.* Vol. 7. "Nebulae and Interstellar Matter." Chicago University of Chicago Press.
31. Kerr, F. J., J. V. Hindman, and B. J. Robinson. 1954. *Australian J. Phys.* 7:297.
32. Kerr, F. J. and G. Westerhout. 1965. In *Stars and Stellar Systems.* Vol. 5. "Galactic Structure." A. Blaauw and M. Schmidt, eds. Chicago: University of Chicago Press.
33. Lin, C. C., C. Yuan, and F. H. Shu. 1969. *Astrophys. J.* 155:721.
34. Madore, B. F. 1971. Unpublished masters thesis. University of Toronto.
35. Madore, B. F.m S. van den Bergh, M. C. H. Wright, and J. E. Baldwin. 1973. In preparation.
36. Mathewson, D. S., P. C. van der Kruit, and W. N. Brouw. 1972. *Astron. Astrophys.* 17:468.
37. Mayall, N. U., and L. H. Aller. 1942. *Astrophys. J.* 95:4.
38. Mestel, L. 1963. *Monthly Notices Roy. Astron. Soc.* 126:553.
39. McGee, R. X. 1964. *I. A. U. Symposium No. 20.* "The Galaxy and the Magellanic Clouds." F. J. Kerr and A. W. Rodgers, eds. Canberra: Australian Academy of Science, p. 126.
40. McGee, R. X. and J. A. Milton. 1966. *Australian J. Phys.* 19:343.
41. Monnet, G. 1971. *Astron. Astrophys.* 12:379.
42. Morgan, W. W. 1958. *Publ. Astron. Soc. Pacific* 70:364.
43. Morgan, W. W. 1959. *Publ. Astron. Soc. Pacific* 71:394.
44. Morgan, W. W. and N. U. Mayall. 1957. *Publ. Astron. Soc. Pacific* 69:291.
45. Oort, J. H. 1964. *I. A. U. Symposium No. 20.* "The Galaxy and the Magellanic Clouds." Canberra: Australian Academy of Science, p. 1.
46. Oort, J. H. 1967. *I. A. U. Symposium No. 31.* "Radio Astronomy and the Galactic System." New York: Academic Press.
47. Pooley, G. G. 1969. *Monthly Notices Roy. Astron. Soc.* 144:101.
48. Roberts, M. S. 1966. *Astrophys. J.* 144:639.
49. Roberts, M. S. 1967. *I. A. U. Symposium No. 31,* Paper 32. New York: Academic Press.
50. Roberts, M. S. 1969. *Astron. J.* 74:859.
51. Robinson, B. J., and J. A. Koehler. 1965. *Nature* 208:993.
52. Rogstad, D. H. 1971. *Astron. Astrophys.* 13:108.
53. Rogstad, D. H., G. W. Rougoor, and J. B. Whiteoak. 1967. *Astrophys. J.* 150:9.
54. Rogstad, D. H. and G. S. Shostak. 1971. *Astron. Astrophys.* 13:99.

55. Rogstad, D. H. and G. S. Shostak. 1972. *Astrophys. J.* 176:315.
56. Rogstad, D. H., G. S. Shostak, and A. H. Rots. 1973. *Astron. Astrophys.* 22:111.
57. Sandage, A. 1961. *Hubble Atlas of Galaxies.* Carnegie Institution of Washington.
58. Sanduleak, N. 1969. *Astrophys. J.* 74:47.
59. Schmidt, M. 1963. *Astrophys. J.* 137:758.
60. Seielstad, G. A., and M. C. H. Wright. 1973. *Astrophys. J.* 184:343.
61. Sersic, J. L. 1960. *Z. Astrophys.* 50:158.
62. Shostak, G. S. 1973. *Astron. Astrophys.* 24:411.
63. Shostak, G. S. 1974. *Astron. Astrophys.* In press.
64. Shostak, G. S. and D. H. Rogstad. 1973. *Astron. Astrophys.* 24:405.
65. Sunyaev, R. A. 1969. *Astrophys. Lett.* 3:33.
66. Vaucouleurs, G. de, and A. de Vaucouleurs. 1964. *eference Catalogue of Bright Galaxies.* Austin: University of Texas Press.
67. Volders, L., and J. A. Högbom. 1961. *Bull. Astron. Inst. Neth.* 15:307.
68. Weinreb, S. 1963. *Technical Report No. 412.* Massachusetts Institute of Technology, Research Laboratory of Electronics.
69. Weliachew, L., and S. T. Gottesman. 1973. *Astron. Astrophys.* 24:59.
70. Wright, M. C. H. 1971a. *Astrophys. J.* 166:455.
71. Wright, M. C. H. 1971b. *Astrophys. Lett.* 7:209.
72. Wright, M. C. H., P. J. Warner, and J. E. Baldwin. 1972. *Monthly Notices Roy. Astron. Soc.* 155:337.
73. Wright, M. C. H. and G. A. Seielstad. 1973. *Astrophys. Lett.* 13:1.